 doi:10.20944/preprints201702.0060.v1

Article

New Protection Scheme for Internal Fault of Multi-Microgrid

Fan Zhang, Longhua Mu * and Wenming Guo

Department of Electrical Engineering, Tongji University, Shanghai 201084, China;
1310491@tongji.edu.cn (F.Z.); gwmsch@163.com (W.G.)
* Correspondence: lhmu@tongji.edu.cn; Tel.: +86-21-59949122

Abstract: Multi-microgrid has many new characteristics, such as bi-directional power flows, flexible operation modes and variable fault currents with different control strategy of inverter interfaced distributed generations (IIDGs). All these featuring aspects pose challenges to multi-microgrid protection. In this paper, current and voltage characteristics of different feeders are analyzed when fault occurs in different positions of multi-microgrid. Based on the voltage and current distribution characteristics of the line parameters, a new protection scheme for the internal fault of multi-microgrid is proposed, which takes the change of phase difference and amplitude of measured bus admittance as the criterion. This scheme with high sensitivity and reliability, has a simple principle and is easy to be adjusted. PSCAD/EMTDC is used in simulation analysis, and simulation results have verified the correctness and effectiveness of the protection scheme.

Keywords: microgrid; multi-microgrid; measured admittance; protection scheme

1. Introduction

Recently, with the escalating energy demand and the pressure to reduce emissions, microgrid has gradually become a hot research topic in power system [1]. Microgrid is the medium or low-voltage power system, which consists of distributed generations (DGs), energy storage device, energy conversion device, loads, corresponding supervision and protection equipment [2, 3]. Multi-microgrid is a new concept of distributed generation network, connecting the microgrids that are geographically adjacent to each other together [4]. Developing the multi-microgrid can not only help to implement the energy complement in different operating conditions among microgrids, but also decrease the system scheduling difficulty. And, in a certain control strategy and energy optimization management, multi-microgrid can improve the self-healing ability of power network, ensuring the continuous power supply to important consumers and increasing the network reliability. Thus, developing multi-microgrid can help to promote better application based on present advantages of microgrids.

One of the key supporting technologies of multi-microgrid is the protection scheme research. The protection scheme of traditional distribution network, including instantaneous trip current protection and overcurrent protection, is designed based on some distinct fault features such as the unidirectional power flow and the high level of fault current. In this scheme, the protection selectivity is achieved by time-delay cooperation. Unlike traditional distribution network, where there is only unidirectional power flow in the power grids; there is bi-directional power flow not only between power grid and multi-microgrid, but also among sub-microgrids. In addition, DGs' currents are usually restricted by fault current limiter [5, 6], and the fault level of multi-microgrid is very low [7, 8]. Given all these considerations, the protection scheme of traditional distribution network cannot be simply transplanted into the multi-microgrid system. Therefore, how to design a protection system for multi-microgrid based on the practiced working condition is a big problem that researchers are very concerned about.

At present, researches on protection of multi-microgrid are just in the early stage. But, some achievements have made on the protection of microgrids.

 doi:10.20944/preprints201702.0060.v1

In [9]-[11] development based on traditional protection algorithms was proposed. Directional comparison longitudinal protection and current differential protection are extended to the protection of microgrids. Differential protection schemes are based on coupled differential directional relays that can accurately locate and isolate faults without affecting other components in distribution systems. But the current differential protection not only needs precise synchronous clock, but also cannot eliminate the influence on differential currents caused by capacitive current and wide area measurement errors. Although directional comparison longitudinal protection doesn't have higher requirements for precise synchronous clock, its sensitivity is low in complex operation conditions of high resistance grounding, system oscillation, power converse, and non-full phase operation.

Adaptive protection was presented in [12]-[14]. Adaptive protection scheme could solve problems arising from both modes of grid connected and islanded operation. In this protection scheme, automatic readjustment of relay settings would be triggered when the microgrid changes from the grid connected mode to the islanded mode. Adaptive protection schemes would automatically adjust the relay settings according to the network operating state. But, it is necessary to install or upgrade the existing protection devices, and it needs the support of fast communication system. Besides, the network topology must be known, which is not flexible. In view of the flexible topology of active distribution network, the adaptive protection has some limitations.

References [15]-[17] proposed the distance protection schemes. The impedance of a line is proportional to its length, thus it is appropriate to use a relay that can measure the impedance of a line up to a predetermined point (the reach point) for distance measurement. Such a relay is called a distance relay and it is designed to operate only for faults that occur between the location of the relay and the selected reach point [18]. But, the measuring precision may be disturbed by harmonics and transient process, and its performance is easily affected by short circuit transition resistance, thus not suitable for short line conditions of the microgrid.

The schemes which have been put forward cannot solve the multi-microgrid protection effectively. The problems mainly display in: (1) Control characteristics of DGs are ignored in most protection schemes, which will have a great impact on the analysis of fault characteristics. (2) The majority of the published papers focus on single microgrid, while the interconnection and interaction among the adjacent microgrids are not taken into consideration.

This paper proposed a new protection scheme for the internal fault of multi-microgrid, which takes into account the control characteristics of DGs and the interconnection and interaction among the adjacent microgrids. By analyzing the current and voltage vector graph before and after the fault, fault characteristics of multi-microgrid can be found and then used to identify the faulty feeders. PSCAD/EMTDC was used in simulation analysis, and simulation results verified the correctness and effectiveness of the protection scheme.

2. Characteristic Analysis of Multi-microgrid

Currently, most of the multi-microgrids as shown in Figure 1 have the medium or low-voltage radial structure [19, 20]. Multi-microgrid is connected to the distribution network through a step-up transformer. In the low-voltage side, there are several AC microgrids with different energy structure and load characteristics. The integration standard of multi-microgrid follows the principles: m sub-microgrids interconnected together at less than 35kV voltage level, with the goal to achieve maximal flow optimization efficiency and minimal power failure efficiency. The multi-microgrid that consists of m sub-microgrids is connected to the distribution network with n interfaces, and $n<m$.

Preprints (www.preprints.org) | NOT PEER-REVIEWED | Posted: 16 February 2017 doi:10.20944/preprints201702.0060.v1

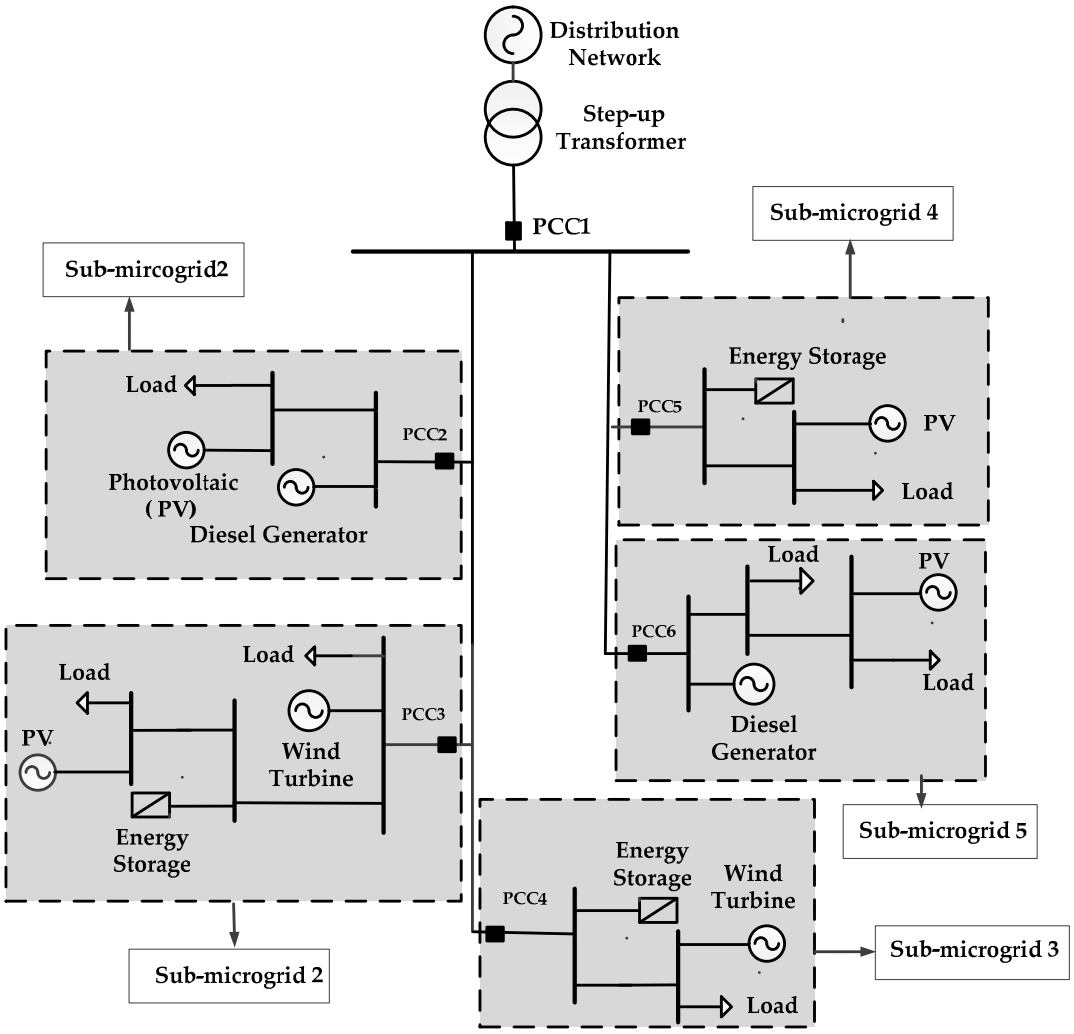

Figure 1. Schematic diagram of multi-microgrid system

Each sub-microgrid is connected to the multi-microgrid via the point of common coupling (PCC). PCC is the connection hub between sub-microgrid and distribution network. By controlling the open and close of PCC, the coordinated control and protection of the whole multi-microgrid can be achieved. The multi-microgrid has three operation modes.

(1)When there is no fault occurring, it operates in grid-connected mode.

(2)If a fault occurs in the distribution network, the multi-microgrid changes into islanded mode.

(3)For the internal fault of multi-microgrid, the faulty sub-microgrid will be switched off, and the others still run in grid-connected mode.

A simplified diagram of Figure 1 is shown as Figure 2. Under grid-connected operation of multi-microgrid, the PCC1 to PCC6 are closed. This paper mainly discusses the protection scheme for the internal fault of the multi-microgrid in grid-connected mode. The feeders in the multi-microgrid are divided into two categories: (1) Double-terminal feeder: the tie line between the sub-microgrid, such as feeders AB, BC, CD, EF, FG, and tie line between two buses, such as the feeders HM, NQ etc. (2) Single-terminal feeder: the feeders connecting to DGs, which are called DG feeders in this paper, including feeders L1 and L3 etc., and the feeders connecting to loads, which are called load feeders, including feeders L2 and L4 etc.

As shown in Figure 2, when faults occur in the double-terminal feeder BC, single-terminal feeders L3 and L2, the change of measured bus admittances before and after fault occurs are analyzed, which are used to identify fault feeder selection criterion.

Preprints (www.preprints.org) | NOT PEER-REVIEWED | Posted: 16 February 2017 doi:10.20944/preprints201702.0060.v1

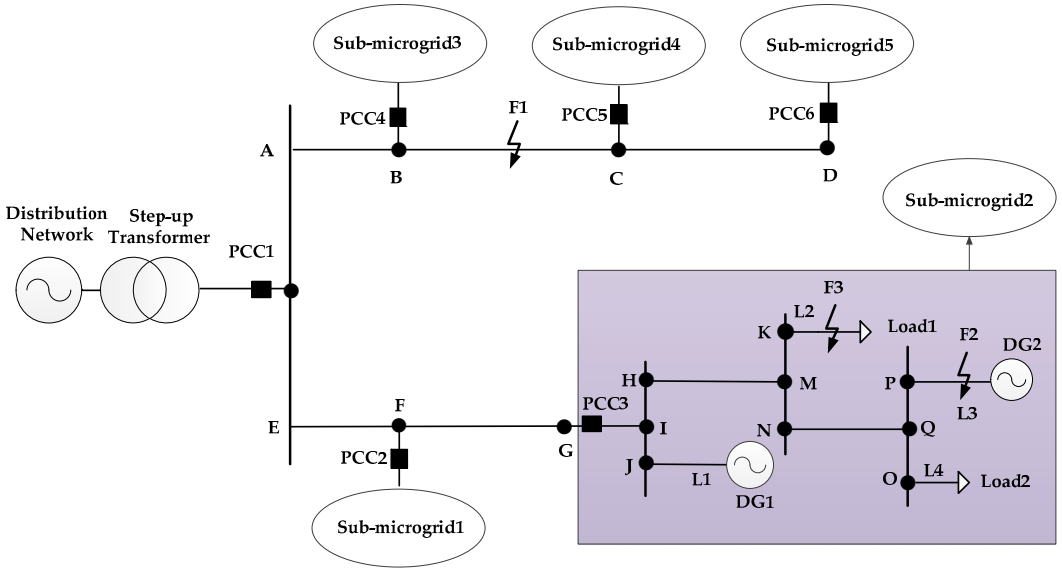

Figure 2. Simplified structure of multi-microgrid system

For purpose of analysis, a simplified line diagram is shown in Figure 3. Set the forward direction of current to be from bus to feeder, and denote $\dot{U}_A$, $\dot{I}_A$, G_A and $\dot{U}_{1A}$, $\dot{I}_{1A}$, G_{1A} as the voltages, currents and measured admittances of A terminal before and after fault occurs. Then, the power flow change of A terminal is defined as four situations.

Figure 3. Current direction of a simplified line

Situation (1): The current direction of A terminal does not change before and after fault occurs, both are in forward direction. The current and voltage vector graphs are shown in Figure 4. The phase of measured admittances of A terminal before and after fault occurs are:

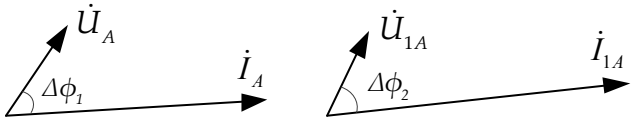

Figure 4. Current and voltage vector graphs of A terminal before and after fault occurs

$$\Delta\phi_1 = arg(G_A) = arg(\dot{I}_A) - arg(\dot{U}_A) \tag{1}$$

$$\Delta\phi_2 = arg(G_{1A}) = arg(\dot{I}_{1A}) - arg(\dot{U}_{1A}) \tag{2}$$

Where arg(·) is the symbol of phase angle. It can be known from Figure 4 that:

$$\begin{cases} -90^o \le \Delta\phi_1 \le 0^o \\ -90^o \le \Delta\phi_2 \le 0^o \end{cases} \tag{3}$$

The phase difference of measured admittances of A terminal before and after fault occurs is:

$$\Delta\phi_A = \Delta\phi_2 - \Delta\phi_1 \tag{4}$$

$$-90^o \le \Delta\phi_A \le 90^o \tag{5}$$

Preprints (www.preprints.org) | NOT PEER-REVIEWED | Posted: 16 February 2017 doi:10.20944/preprints201702.0060.v1

Situation (2): The current direction of A terminal does not change. Both are in reverse direction. The current and voltage vector graph is shown in Figure 5.

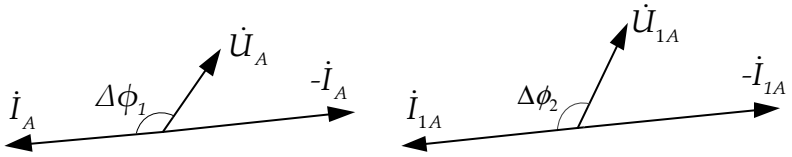

Figure 5. Current and voltage vector graphs of A terminal before and after the fault

It can be known from Figure 5 that:

$$\begin{cases} 90^o \le \Delta\phi_1 \le 180^o \\ 90^o \le \Delta\phi_2 \le 180^o \end{cases} \tag{6}$$

The phase difference of measured admittances of A terminal before and after the fault occurrence is:

$$\Delta\phi_A = \Delta\phi_2 - \Delta\phi_1 \tag{7}$$

So: $$-90^o \le \Delta\phi_A \le 90^o \tag{8}$$

Situation (3): The current direction of A terminal is forward before the fault occurrence, and reverse after the fault occurrence. The current and voltage vector graphs are shown in Figure 6.

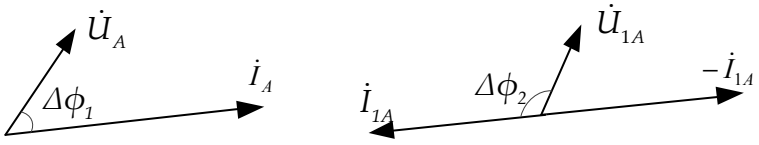

Figure 6. Current and voltage vector graphs of A terminal before and after the fault

It can be known from Figure 6 that:

$$\begin{cases} -90^o \le \Delta\phi_1 \le 0^o \\ 90^o \le \Delta\phi_2 \le 180^o \end{cases} \tag{9}$$

The phase difference of measured admittances of A terminal before and after the fault occurrence is:

$$\Delta\phi_A = \Delta\phi_2 - \Delta\phi_1 \tag{10}$$

So $$90^o \le \Delta\phi_A \le 270^o \tag{11}$$

Situation (4): The current direction of A terminal is reverse before the fault, and forward after the fault. The current and voltage vector graph is shown in Figure 7.

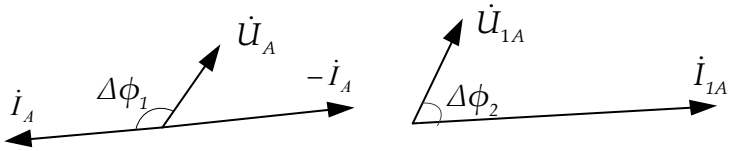

Figure 7. Current and voltage vector graph of A terminal before and after the fault

It can be known from Figure 7 that:

$$\begin{cases} 90^o \le \Delta\phi_1 \le 180^o \\ -90^o \le \Delta\phi_2 \le 0^o \end{cases} \tag{12}$$

The phase difference of measured admittance of A terminal before and after the fault is:

$$\Delta\phi_A = \Delta\phi_2 - \Delta\phi_1 \tag{13}$$

Preprints (www.preprints.org) | NOT PEER-REVIEWED | Posted: 16 February 2017 doi:10.20944/preprints201702.0060.v1

So $$90^o \le \Delta\phi_A \le 270^o \quad (14)$$

Based on the above analysis, the phase difference change information of measured admittance of *A* terminal before and after the fault occurs is available, as shown in Table 1.

Table 1. Phase difference change information of measured admittance of *A* terminal before and after the fault

Direction / Measured Admittance	Forward-forward Situation(1)	Reverse-reverse Situation (2)	Forward-reverse Situation(3)	Reverse-forward Situation (4)
Phase Difference	-90⁰~90⁰	-90⁰~90⁰	90⁰~270⁰	90⁰~270⁰

3. Fault Analysis

3.1. Fault occurs in Double-terminal Feeder

3.1.1. Fault Analysis for the Fault Double-terminal Feeder

The fault analysis for fault occurring in double-terminal feeder takes the F1-fault in line BC as an example. In the case of normal operation, the power flow of feeder BC consists of the following two situations.

(a)The load demand of sub-microgrid 4 and 5 is greater than the generation capacity of DGs; the power flow is from the *B* terminal to *C* terminal.

(b)The load demand of sub-microgrid 4 and 5 is less than the generation capacity of DGs; the power flow is from the *C* terminal to *B* terminal.

Situation (a): Suppose $\dot{U}_B$, $\dot{I}_B$ and $\dot{U}_{1B}$, $\dot{I}_{1B}$ are the voltages and currents of *B* terminal in line BC before and after fault occurs. For *B* terminal, it is in the upstream of the fault point, and connected with distribution network, so the voltage will basically remain unchanged when fault happens, but the current will increase markedly. The variation of current and voltage before and after fault are:

$$\left|\dot{U}_{1B}\right| \le \left|\dot{U}_B\right| \quad (15)$$

$$\left|\dot{I}_B\right| << \left|\dot{I}_{1B}\right| \quad (16)$$

The measured admittances of *B* terminal before and after fault occurs are:

$$G_B = \dot{I}_B / \dot{U}_B \quad (17)$$

$$G_{1B} = \dot{I}_{1B} / \dot{U}_{1B} \quad (18)$$

Combining (15) to (18), it can be known that the measured admittance amplitude is:

$$\left|G_{1B}\right| >> \left|G_B\right| \quad (19)$$

Before and after the fault occurs, the current directions of *B* terminal are both forward direction. It can be known from Table 1 that the phase difference of measured admittance of *B* terminal is:

$$-90^o \le \Delta\phi_B \le 90^o$$

After the fault occurs, the DGs in the downstream of *C* terminal cannot provide enough short circuit capacity, so the voltage of *C* terminal will drop dramatically. Also, the DGs in the sub-microgrids are inverter interfaced distributed generators (IIDG), which are usually under PQ control strategy with low voltage ride-through capability. When the voltage of the fault point drops a lot, the output current of the IIDG may reverse, and decrease in amplitude [21]. So the measured admittance amplitude change of *C* terminal before and after the fault occurs cannot be estimated directly with formula (17) and (18).

Before fault occurs, the current direction of *C* terminal is reverse. When fault occurs, it turns to forward. So the phase difference of measured admittance of *C* terminal is:

Preprints (www.preprints.org) | NOT PEER-REVIEWED | Posted: 16 February 2017 doi:10.20944/preprints201702.0060.v1

$$90^o \le \Delta\phi_C \le 270^o$$

Situation (b): In this case, the change information of measured admittance amplitude of *B* terminal is just the same with formula (19). Before fault occurs, the current direction of *B* terminal is reverse. When fault occurs, it turns to forward direction. So the phase difference of measured admittance of *B* terminal is:

$$-90^o \le \Delta\phi_B \le 90^o$$

Before and after fault occurs, the current directions of *C* terminal are both forward. So the phase difference of measured admittance of *C* terminal is:

$$-90^o \le \Delta\phi_C \le 90^o$$

3.1.2. Fault Analysis for the Healthy Double-terminal Feeder

For fault occurs in F1, the analysis for healthy double-terminal feeders takes line AB as an example. Before fault occurs, the power flow of line AB consists of the following two situations.

(a) The load demand of sub-microgrid 3, 4 and 5 is greater than the generation capacity of DGs; the power flow is from the *A* terminal to *B* terminal.

(b) The load demand of sub-microgrid 3, 4 and 5 is less than the generation capacity of DGs; the power flow is from the *B* terminal to *A* terminal.

Situation (a): Suppose G_A, G_{1A} and G_B, G_{1B} are the measured admittances of *A* and *B* terminal before and after fault occurs. In this case, *A* and *B* terminals are also in the upstream of the fault point, and connecting with distribution network, so the voltage will basically remain unchanged when fault happens, but the current will increase markedly. Then, it can be got:

$$|G_{1A}| >> |G_A|$$

$$|G_{1B1}| >> |G_{1B}|$$

Before and after the fault occurs, the current directions of *A* terminal are both forward, while current directions of *B* terminal are both reverse. So the phase differences of measured admittance of *A* and *B* terminal are:

$$-90^o \le \Delta\phi_A \le 90^o$$

$$-90^o \le \Delta\phi_B \le 90^o$$

Situation (b): *A* and *B* terminals are in the upstream of the fault point, so it's easy to derive that:

$$|G_{1A}| >> |G_A|$$

$$|G_{1B1}| >> |G_{1B}|$$

Before fault occurs, the current direction of *A* terminal is reverse, but for *B* terminal, it is forward direction. When fault occurs, the current of *A* terminal turns to forward direction. And it is reverse direction for *B* terminal. So the phase differences of measured admittance of *A* and *B* terminal are:

$$90^o \le \Delta\phi_A \le 270^o$$

$$90^o \le \Delta\phi_B \le 270^o$$

The power flow analysis for other healthy double-terminal feeders is similar to the feeder AB, they won't be covered here.

Preprints (www.preprints.org) | NOT PEER-REVIEWED | Posted: 16 February 2017 doi:10.20944/preprints201702.0060.v1

3.1.3. Fault Analysis for Single-terminal Feeder

In this case, the current and voltage will basically remain unchanged, thus the measured admittance amplitude of them will be almost not changed, after the fault occurs.

For the DG feeders, the current directions of them are from DGs to the upstream bus, and are all reverse direction. So the phase difference of measured admittance is:

$$-90^o \le \Delta\phi_{DG} \le 90^o$$

For the load feeders, the current directions of them are from the upstream bus to the loads, and are all forward directions. So the phase difference of measured admittance is:

$$-90^o \le \Delta\phi_{Load} \le 90^o$$

3.2. Fault Occurs in Single-terminal Feeder

The analysis for fault occurs in single-terminal feeder takes the F2-fault of feeder L3 and F3-fault of feeder L2 as examples.

3.2.1. Fault Occurs in F2

For the fault occurs in F2, as shown in Figure 2, DG2 is connected to the feeder L3, and *P* terminal is the access point that L3 connects with the upstream bus. Before the fault occurs, the current direction of *P* terminal is from DG2 to the upstream bus, it is reverse direction. But after fault occurs, it is from the upstream bus to fault point, and changes into forward direction. So the phase difference of measured admittance is:

$$90^o \le \Delta\phi_P \le 270^o$$

The power flow analysis for the other healthy other feeders are the same with the feeder in the previous chapter 3.1, so no repeated analysis is discussed.

3.2.2. Fault Occurs in F3

For the fault occurs in F3, as shown in Figure 2, load2 is connected to the feeder L2, and *K* terminal is the access point that L2 connects with the upstream bus. Before and after the fault occurs, the current direction of *K* terminal is from the upstream bus to fault point, and are all forward direction. So the phase difference of measured admittance is:

$$-90^o \le \Delta\phi_K \le 90^o$$

K terminal is in the upstream of the fault point, so the measured admittance amplitude of *K* terminal will increase markedly after the fault occurs. But for the other feeders that connects with loads, the current and voltage will basically remain unchanged, thus the measured admittance amplitude of them will be almost not changed, after the fault occurs.

The power flow analysis for the other feeders are also similar to the feeders in the previous chapter 3.1, so no repeating analysis is discussed.

4. Protection Scheme for Internal Fault of Multi-microgrid

4.1. Criterion for Fault Locating

Based on the above analysis, the change information of measured admittances for multi-microgrid before and after fault occurs are concluded in Table 2.

Preprints (www.preprints.org) | NOT PEER-REVIEWED | Posted: 16 February 2017 doi:10.20944/preprints201702.0060.v1

Table 2. Change information of measured admittance

Fault Position / Measured Admittance			F1		F2		F3	
			$\Delta\phi$	$\lvert G_i \rvert$	$\Delta\phi$	$\lvert G_i \rvert$	$\Delta\phi$	$\lvert G_i \rvert$
Double-terminal Feeder		Fault	90^0~270^0 and -90^0~90^0	Increases Significantly	—	—	—	—
		Healthy	90^0~270^0 or -90^0~90^0	Basically Unchanged	90^0~270^0 or -90^0~90^0	Basically Unchanged	90^0~270^0 or -90^0~90^0	Basically Unchanged
Single-terminal Feeder	DG Feeder	Fault	—	—	90^0~270^0	Increases Significantly	—	—
		Healthy	-90^0~90^0	Basically Unchanged	-90^0~90^0	Basically Unchanged	-90^0~90^0	Basically Unchanged
	Load Feeder	Fault	—	—	-90^0~90^0	Basically Unchanged	-90^0~90^0	Increases Significantly
		Healthy	-90^0~90^0	Basically Unchanged	—	—	-90^0~90^0	Basically Unchanged

By analyzing the change of the measured admittances before and after fault occurs, the following results are obtained:

(1) Fault occurs in double-terminal feeder

The phase difference of measured admittance of the two terminals is in the range 90^0~270^0 and -90^0~90^0 respectively. For the healthy double-terminal feeders, the phase difference of the two terminals are both in the range 90^0~270^0 or -90^0~90^0. For the single-terminal feeders, the phase difference range are all in -90^0~90^0.

(2) Fault occurs in single-terminal feeder

If the fault occurs in the DG feeders, the phase difference of measured admittance is in the range 90^0~270^0. For the double-terminal feeder, the phase difference are both in the range 90^0~270^0 or -90^0~90^0. For the other single-terminal feeder, the phase difference range are all -90^0~90^0. If fault occurs in the load feeders, the phase difference of double-terminal feeders are both in the range 90^0~270^0 or -90^0~90^0. For the single-terminal feeders, the phase difference range are all -90^0~90^0.

From the above analysis, it will be easy to get some solution to identify the faulty feeder only by the change of the phase difference of measured admittance, when the fault occurs in DG feeders or double-terminal feeders. But for the fault in the load feeders, there is no obvious fault feature for the change of the phase difference of measured admittance, which is in the same range before and after the fault. For the load feeders, based on the above analysis, it can be known that there is only load connected, and its power is only provided by the upstream bus. When the fault occurs, the current of it will increase significantly, and the voltage will drop dramatically. The measured admittance amplitude will largely increase; therefore, it can be selected as the fault criterion for the load feeders.

Overall, the following fault criterions are concluded to detect the internal fault of multi-microgrid.

Criterion 1: DG Feeders. The phase difference of measured admittance is:

$$90^o \le \Delta\phi_1 \le 270^o$$

Criterion 2: Double-terminal feeder. The phase difference of measured admittance is: the range of one terminal is -90°~90°, the other terminal is 90°~270°. That is:

$$-90^o \le \Delta\phi_2 \le 90^o$$

$$90^o \le \Delta\phi_3 \le 270^o$$

Preprints (www.preprints.org) | NOT PEER-REVIEWED | Posted: 16 February 2017 doi:10.20944/preprints201702.0060.v1

Criterion 3: Load feeders. The measured admittance amplitude of load feeders largely increase after the fault, and exceeds a particular threshold G_{set}, which is 4~5 times bigger before fault occurs.

4.2. The Protection Scheme of Multi-microgrid

The flow chart of protection scheme is shown in Figure 8.

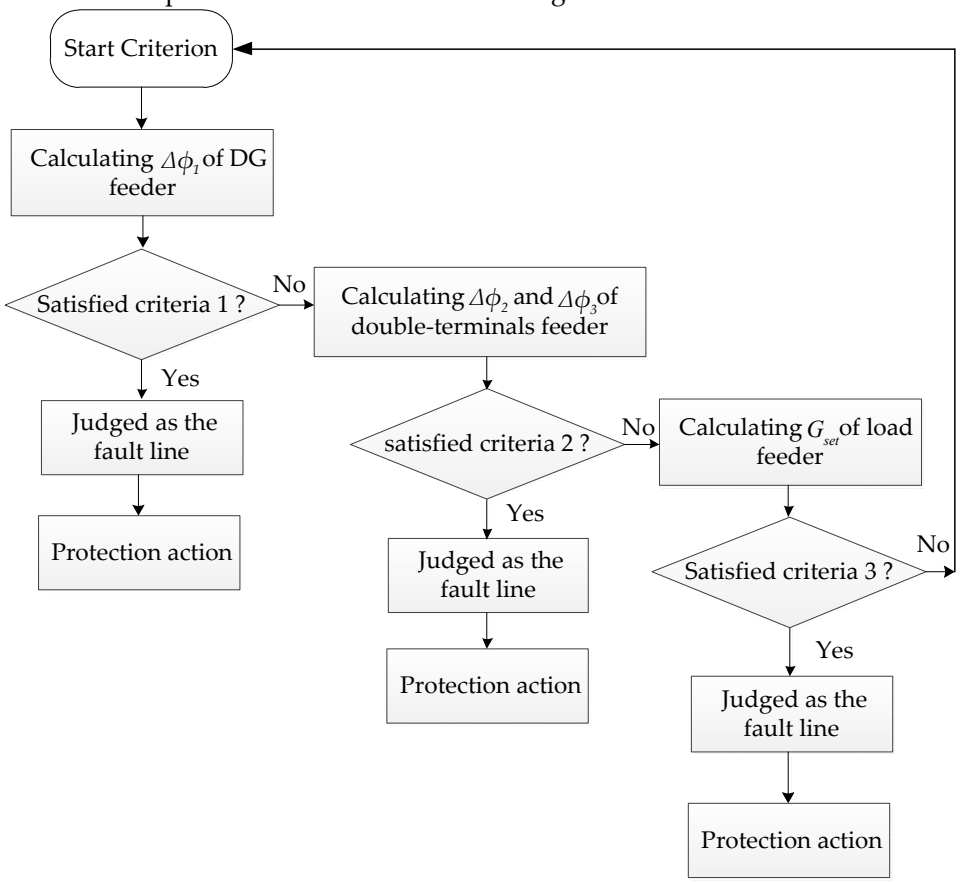

Figure 8. Flow chart of protection scheme

The basic process is described as follows:

(1) When the start criterion is satisfied, the phase difference of measured admittance $\Delta\phi_1$ of DG feeders is calculated. When the criteria 1 is met, the DG feeder is judged as the fault line.

(2) If the criteria 1 is not satisfied, then the phase difference of measured admittance $\Delta\phi_2$ and $\Delta\phi_3$ of double-terminal feeders is calculated. When the criteria 2 is met, the feeder is judged as the fault line.

(3) If the criteria 2 is not met, the measured admittance amplitude of load feeders is calculated. When the criteria 3 is met, the load feeder is judged as the fault line.

(4) Protection actions and fault feeder is removed.

5. Simulation Results

To validate the effectiveness and feasibility of the proposed method, a multi-microgrid with a high amount of DGs is established in PSCAD/EMTDC.

As shown in Figure 9, the multi-microgrid consists of three 10kV sub-microgrids, and is connected to the main 35kV distribution network through a step-up transformer. The capacity and frequency of system is 100MVA and 50Hz. The DGs in each sub-microgrid are based on the fault model of IIDG under PQ control strategy with low voltage ride-through capability. The capacity of DGs and loads in each sub-microgrid are shown in Table 3. For the purposes of analysis, each sub-microgrid consists of one DG. Positive-sequence resistance and reactance of the feeders are 0.38Ω/km and 0.45Ω/km and zero-sequence resistance and reactance are 0.76Ω/km and 1.32Ω/km.

Preprints (www.preprints.org) | NOT PEER-REVIEWED | Posted: 16 February 2017 doi:10.20944/preprints201702.0060.v1

Intelligent electronic devices (IEDs) are installed at the beginning of the single-terminal feeders. For double-terminal feeder IEDs are installed at the two terminals of each line respectively.

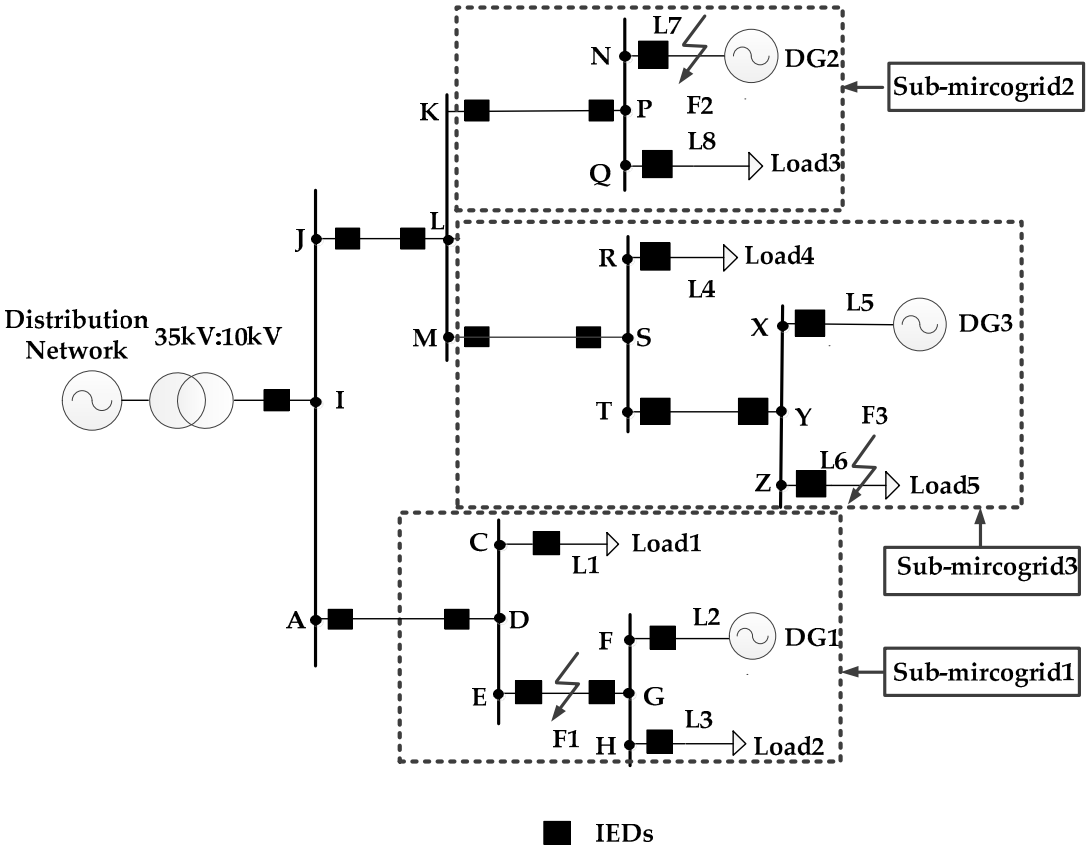

Figure 9. Simulation model of multi-microgrid

Table 3. Capacity of DGs and loads in multi-microgrid

Number of Multi-microgrid	Loads	DGs
1	LD1:(1500+15j)kVA LD2: (1200+30j)kVA	DG1:500kW
2	LD3: (1200+30j)kVA	DG2: 400kW
3	LD4: (1200+30j)kVA LD5: (900+27j)kVA	DG3:600kW

Three fault points namely F1, F2 and F3 are selected to show faults occurring in different sections of the multi-microgrid. F1 fault occurs in the double-terminal feeder EG; F2 fault occurs in the DG feeder L7 that connects with DG2; F3 fault occurs in the load feeder L6 that connects with load5. The above three fault points can reflect the overall fault location well. The phase-phase ground fault is selected as fault type and faults occur at 0.3s after the simulation starts. The transition resistance of the fault point is 2Ω. The amplitude and phase difference change information of measured admittance before and after the fault occurs are analyzed.

5.1. Fault occurs at F1

Measured admittance results of the multi-microgrid before the fault occurs are shown in Table 4. When F1 fault occurs, the measured admittance results of multi-microgrid are shown in Table 5. Figure 10 shows the phase difference of measured admittance change information of *E* and *G* terminals. $\Delta\phi_i$, $|G_i|$ and $\Delta\phi_{1i}$, $|G_{1i}|$ are the phase and amplitude of measured admittance before and after the fault occurs respectively. $\Delta\phi$ is the phase difference of the measured admittance.

Preprints (www.preprints.org) | NOT PEER-REVIEWED | Posted: 16 February 2017 doi:10.20944/preprints201702.0060.v1

In this case, it can be seen from Table 4, 5 and Figure 10 that before and after the fault occurs, the phase difference of the measured admittance of *E* and *G* terminal are -48.64^0 and 150.99^0 respectively, and satisfies the criterion 2. For the other double-terminal feeders, the phase difference of measured admittance of the two terminals is both in the range -90^0~90^0, so the criterion 2 is not satisfied. For the DG feeders, the phase difference of the measured admittance of each terminal is in the range -90^0~90^0, and the criterion 1 is not satisfied. And for the load feeders, the amplitude of the measured admittances are almost unchanged, and the criterion 3 is not satisfied. Thus, the feeder EG is judged as the fault line.

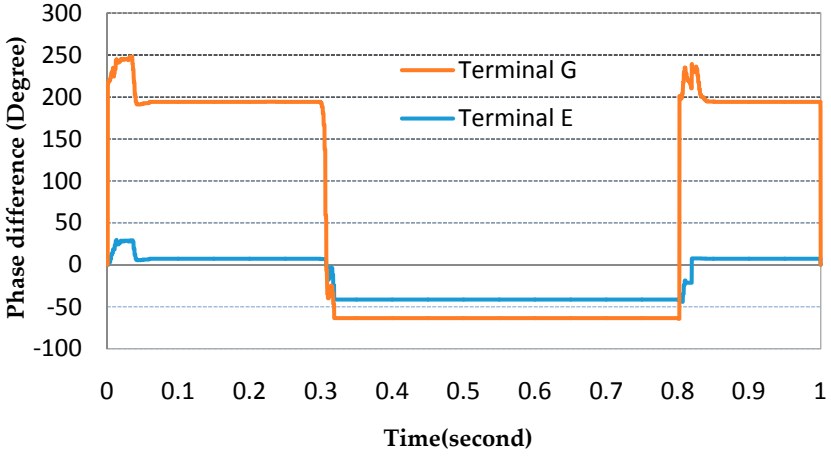

Figure 10. The measured admittance amplitude change information of E terminal

Table 4. Measured admittance results before fault occurs

Feeder	Terminal	$\|G_i\|$	$\Delta\phi_i\,(o)$	Feeder	Terminal	$\|G_i\|$	$\Delta\phi_i\,(o)$
EG	*E*	0.004	7.14	L5	*X*	0.003	172.92
	G	0.004	186.89	L6	*Z*	0.009	-1.76
L1	*C*	0.015	-1.13	L7	*N*	0.006	175.1
L2	*F*	0.015	173.82	TY	*T*	0.006	-1.93
L3	*H*	0.012	-1.49		*Y*	0.006	176.92
L4	*R*	0.012	175.02	L8	*Q*	0.012	-1.66
KP	*K*	0.006	170.21	AD	*A*	0.019	-0.4
	P	0.006	-2.03		*D*	0.019	174.68
JL	*J*	0.023	-1.81	MS	*M*	0.017	-1.94
	L	0.023	176.1		*S*	0.017	177.9

Table 5. Measured admittance results when F1 fault occurs

Feeder	Terminal	$\Delta\phi_i\,/(o)$	$\Delta\phi\,/(o)$	$\|G_{1i}\|$	Feeder	Terminal	$\Delta\phi_i\,/(o)$	$\Delta\phi\,/(o)$	$\|G_{1i}\|$
EG	*E*	-41.50	-48.64	1.467	L5	*X*	158.67	-14.25	0.004
	G	-22.12	150.99	0.149	L6	*Z*	-1.54	0.22	0.009
L1	*C*	-1.12	0.01	0.015	L7	*N*	171.36	-3.74	0.008
L2	*F*	156.15	-17.67	0.015	TY	*T*	-15.32	-13.39	0.006
L3	*H*	-1.54	-0.05	0.012		*Y*	172.58	-4.34	0.006
L4	*R*	158.67	-16.35	0.012	L8	*Q*	-1.76	-0.1	0.012
KP	*K*	140.45	-29.76	0.007	AD	*A*	-34.7	-34.3	0.729
	P	-20.16	-18.13	0.007		*D*	138.88	-35.8	1.479
JL	*J*	-19.35	-17.54	0.025	MS	*M*	-10.58	-8.64	0.018
	L	160.82	-15.28	0.024		*S*	169.23	-8.67	0.018

Preprints (www.preprints.org) | NOT PEER-REVIEWED | Posted: 16 February 2017 doi:10.20944/preprints201702.0060.v1

5.2. Fault occurs at F2

When fault occurs at F2, the measured admittance results of the multi-microgrid are shown in Table 6. Figure 11 shows the phase difference of measured admittance change information of N terminal.

In this case, it can be seen from Table 6 and Figure 11 that before and after the fault occurs, the phase difference of the measured admittance of *N* terminal is 167.32^0, and the criterion 1 is satisfied. For the double-terminal feeders, the phase difference of the measured admittance of the two terminals are both in the range -90^0~90^0, so the criterion 2 is not satisfied. For the other DG feeders, the phase difference of the measured admittance of each terminal is in the range -90^0~90^0, and the criterion 1 is not satisfied. And for the load feeders, the amplitude of the measured admittances are almost unchanged, so the criterion 3 is not satisfied. Thus, the feeder L7 is judged as the fault line.

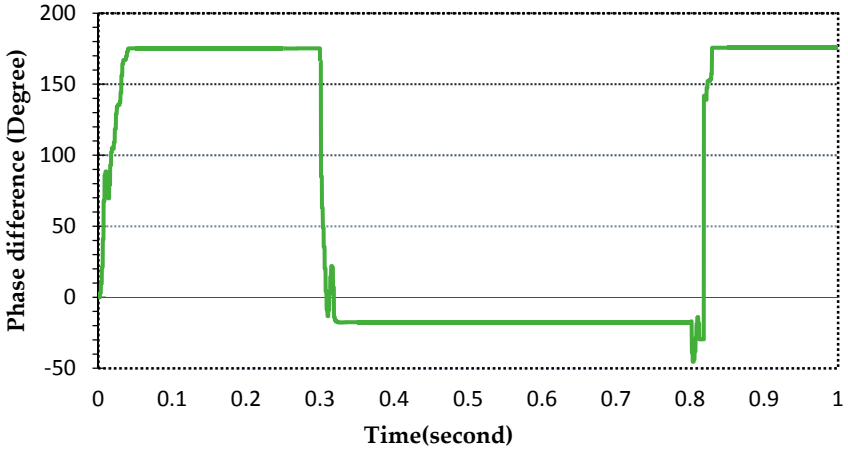

Figure 11. The measured admittance difference change information of *N* terminal

Table 6. Measured admittance results when F2 fault occurs

Feeder	Terminal	$\Delta\phi_i/(o)$	$\Delta\phi/(o)$	$\lvert G_{1i}\rvert$	Feeder	Terminal	$\Delta\phi_i/(o)$	$\Delta\phi/(o)$	$\lvert G_{1i}\rvert$
EG	*E*	-27.42	-34.56	0.008	L5	*X*	166.32	-6.6	0.031
	G	155.63	-30.76	0.008	L6	*Z*	-1.77	-0.01	0.009
L1	*C*	-1.12	0.01	0.015	L7	*N*	-17.58	167.32	6.718
L2	*F*	154.84	-18.98	0.015	TY	*T*	-68.12	-66.19	0.031
L3	*H*	-1.59	-0.1	0.012		*Y*	109.4	-67.52	0.029
L4	*R*	158.67	-16.35	0.013	L8	*Q*	-1.55	0.11	0.012
KP	*K*	160.4	-9.81	6.28	AD	*A*	-17.18	-16.78	0.02
	P	-19.65	-17.62	6.729		*D*	163.28	-11.4	0.02
JL	*J*	-44.69	-42.88	0.958	MS	*M*	-55.63	-53.69	0.039
	L	144.56	-31.54	6.284		*S*	131.26	-46.64	0.03

5.3. Fault occurs at F3

When fault occurs at F3, the measured admittance results of the multi-microgrid are shown in Table 7. The measured admittance amplitude change information of *Z* terminal is shown in Figure 12.

In this case, it can be seen from Figure 12 and Table 7 that the measured admittance amplitude of Z terminal is 0.009 before the fault occurs. It changes into 6.587 after the fault occurs, and increases about 730 times, so the criterion 3 is satisfied. And for the other load feeders, the amplitude of the measured admittances are almost unchanged, so the criterion 3 is not satisfied.

Preprints (www.preprints.org) | NOT PEER-REVIEWED | Posted: 16 February 2017 doi:10.20944/preprints201702.0060.v1

The phase difference of the measured admittance of the double-terminal feeders are both in the range -90⁰~90⁰, so the criterion 2 is not satisfied. For the DG feeders, the phase difference of the measured admittances of each terminal is in the range -90⁰~90⁰, and the criterion 1 is not satisfied. Thus, the feeder L6 is judged as the fault line.

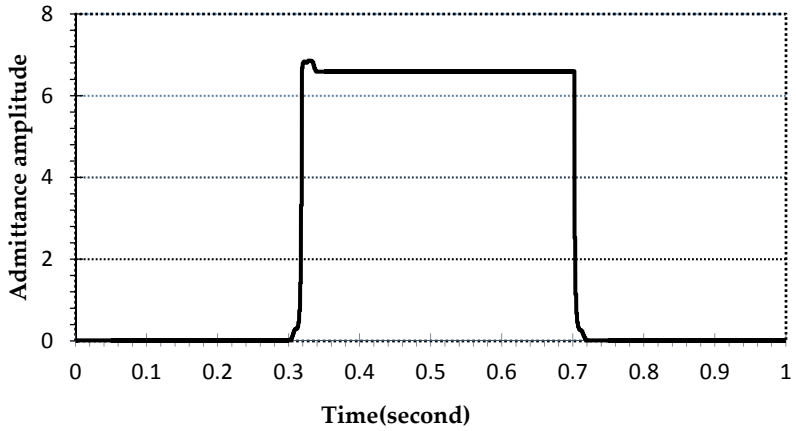

Figure 12. The measured admittance amplitude change information of *N* terminal

Table 7. Measured admittance results when F3 fault occurs

Feeder	Terminal	$\Delta\phi_i/(o)$	$\Delta\phi/(o)$	$\lvert G_{1i}\rvert$	Feeder	Terminal	$\Delta\phi_i/(o)$	$\Delta\phi/(o)$	$\lvert G_{1i}\rvert$
EG	*E*	-24.7	-31.84	0.006	L5	X	145.62	-27.3	0.116
	G	155.43	-30.39	0.006	L6	Z	-1.65	0.11	6.587
L1	*C*	-1.31	-0.18	0.015	L7	N	161.23	-13.87	0.011
L2	*F*	166.83	-6.99	0.015	TY	T	-46.36	-44.43	0.703
L3	*H*	-1.49	0	0.012		Y	162.86	-14.12	6.56
L4	*R*	141.91	-33.11	0.012	L8	Q	-18.07	-16.41	0.012
KP	*K*	166.34	-3.87	0.009	AD	A	-8.86	-8.46	0.02
	P	-12.36	-10.33	0.009		D	173.24	-1.48	0.02
JL	*J*	-44.35	-42.54	0.278	MS	M	-44.52	-42.58	0.703
	L	139.79	-36.31	0.374		S	137.56	-40.4	0.376

From the above simulation results, it can be seen that the fault situations are consistent with the theoretical analysis in chapter 3. Fault location can be determined by the protection criterions in chapter 4. Thus, the fault line will be removed in time, and the protection function can be achieved.

6. Conclusions

A new protection scheme for internal fault of multi-microgrid is proposed in this paper, which takes into account the control characteristics of DGs and the interconnection and interaction among adjacent microgrids. Current and voltage characteristics of different feeders are analyzed when fault occurs in different positions of multi-microgrid. Fault location is realized by comparing the phase difference and amplitude of measured admittance of the feeders. The change of the measured bus admittance is the result of joint action of voltage and current, and the change of the measured admittance amplitude before and after the fault occurs is obvious and defined as the protection criterion for the load feeders. Meanwhile, the phase difference of the measured admittance is defined as another protection criterion for the double-terminal and DG feeders. It is not a fixed value, but a phase interval. And large redundancy is introduced in the derivation of the protection criterion. Fault occurs in different feeders of multi-microgrid can be effectively distinguished. Thus, the detection and location of the fault can be implemented.

A multi-microgrid which consists of three 10kV sub-microgrids is established in PSCAD/EMTDC. To examine the efficiency of the protection scheme, the phase-phase ground fault is simulated at three points. Theoretical analysis and system simulation results demonstrate the superiority and accuracy of the proposed scheme.

Acknowledgments: This work was supported in part by National Fundamental Research (973) Program of China (2014CB249201).

Author Contributions: The paper was a collaborative effort among the authors. Fan Zhang performed the simulation, analyzed the data, and wrote the paper. Longhua Mu provided critical comments. Wenming Guo supervised the related research work.

Conflicts of Interest: The authors declare no conflict of interest.

References

1. Laaksonen H J. Protection principles for future microgrids. *IEEE Trans. Power Electron* **2011**, 25, 2910-2918.
2. A. Solanki; A. Nasiri; V. Bhavaraju; Y. L. Familiant and Q. Fu. A New Framework for Microgrid Management: Virtual Droop Control. *IEEE Trans. Smart Grid* **2016**, 7, 554-566.
3. Olivares D E; Mehrizi-Sani A; Etemadi A H, et al. Trends in microgrid control. *IEEE Trans. Smart Grid* **2014**, 5, 1905-1919.
4. Zhao M; Chen Y; Shen C and Huang X Q. Characteristic analysis of multi-microgrids and a pilot project design. *Power sys techno*. **2015**, 39, 1469-1476.
5. Rajaei N; Ahmed M H; Salama M M A, et al. Fault current management using inverter-based distributed generators in smart grids. *IEEE Trans. Smart Grid* **2014**, 5, 2183-2193.
6. Camacho A; Castilla M; Miret J, et al. Active and reactive power strategies with peak current limitation for distributed generation inverters during unbalanced grid faults. *IEEE Trans. Ind. Electron* **2015**, 62, 1515-1525.
7. Zamani M A; Yazdani A; Sidhu T S. A control strategy for enhanced operation of inverter-based microgrids under transient disturbances and network faults. *IEEE Trans. Power Del* **2012**, 27, 1737-1747.
8. Lopes J A P; Moreira C L; Madureira A G. Defining control strategies for microgrids islanded operation. *IEEE Trans. Power Syst* **2006**, 21, 916-924.
9. Zhang B; Hao Z; Bo Z. New development in relay protection for smart grid. *Protection & Control of Modern Power Systems* **2016**, 1, 2109-2118.
10. Jing L; Son D H; Kang S H, et al. A novel protection method for single line-to-ground faults in ungrounded low-inertia microgrids. *Energies* **2016**, 9, 1031.
11. E. Casagrande; W. L. Woon; H. H. Zeineldin and D. Svetinovic. A differential sequence component protection scheme for microgrids with inverter-based distributed generators. *IEEE Trans. Smart Grid* **2014**, 5, 29-37.
12. Laaksonen H; Ishchenko D; Oudalov A. Adaptive protection and microgrid control design for Hailuoto island. *IEEE Trans. Smart Grid* **2014**, 5, 1486-1493.
13. L. Che; M. E. Khodayar and M. Shahidehpour. Adaptive protection system for microgrids: Protection practices of a functional microgrid system. *IEEE Commun. Mag*. **2014**, 2, 66-80.
14. Sukumar M B; Adly A G. Development of adaptive protection scheme for distribution systems with high penetration of distributed generation. *IEEE Trans. Power Del* **2004**, 19, 56-63.
15. W. Huang; T. Nengling; X. Zheng; C. Fan; X. Yang and B. J. Kirby. An impedance protection scheme for feeders of active distribution networks. *IEEE Trans. Power Del* **2014**, 29, 1591-1602.
16. S. Mirsaeidi; D. Mat Said; M. W. Mustafa and M. Hafiz Habibuddin. A protection strategy for micro-grids based on forward-sequence component. *IET Renew. Power Gener*. **2015**, 9, 600-609.
17. Dewadasa M; Ghosh A; Ledwich G, et al. Fault isolation in distributed generation connected distribution networks. *IET Gener. Transm. Distrib*. **2011**, 5, 1053-1061.
18. Mirsaeidi S; Said D M; Mustafa M W, et al. Progress and problems in micro-grid protection schemes. Renew Sustain Energy Rev. **2014**, 37, 834-839.
19. B. Kroposki; R. Lasseter; T. Ise, et al. Making microgrid work. *IEEE Commun. Mag*. **2008**, 3, 40-53.
20. Soshinskaya M; Crijns-Graus W H J; Guerrero J M, et al. Microgrids: Experiences, Barriers and Success Factors. *Renew. Sust. Energ. Rev*. **2014**, 40, 659-672.

21. Han H J; Mu L H; Guo W M. Adaptability of microgrid protection based on fault components. *Automat Electron Power Sys*. **2016**, 40, 90-96.